*Korean J. Chem. Eng.*, 36(11), 1859-1868 (2019)
DOI: 10.1007/s11814-019-0375-y

pISSN: 0256-1115
eISSN: 1975-7220

# Energy saving in carbon dioxide hydrate formation process using Boehmite nanoparticles

**Vahab Montazeri*, Masoud Rahimi*,†, and Bahman Zarenezhad****

*Department of Chemical Engineering, Razi University, Kermanshah, Iran
**Faculty of Chemical, Petroleum and Gas Engineering, Semnan University, Semnan, Iran
(*Received 13 March 2019 • accepted 28 August 2019*)

**Abstract**–This work reports on an attempt to save energy in the carbon dioxide hydrate formation process. The kinetics of carbon dioxide hydrate formation induced by synthesized Boehmite (AlOOH) nanoparticles was investigated at 274.15 K, different initial pressures (29, 32 and 35 bar), impeller speed (50, 100 and 200 rpm) and AlOOH concentrations (25, 50 75, 100, 200 ppm). It was also observed that there is a desirable concentration for AlOOH nanoparticles in which the maximum rate of gas consumption and minimum growth and induction time was obtained. According to the results at 29 bar and 100 rpm and in the presence of 50 ppm AlOOH, the gas consumption rate increased to 150%, while the induction time and growth time decreased about 82.8% and 46.1%, respectively. The maximum energy saving of 49.7% for 50 ppm AlOOH was observed, which is very important for industrial applications of carbon dioxide hydrate. The presented technique is useful for intensification of gas hydrate-based $CO_2$ capture processes in the oil and gas industry with minimum energy consumption.

Keywords: Energy Saving, $CO_2$ Capture, Nanoparticles, Hydrate, Kinetics, Boehmite

## INTRODUCTION

Greenhouse gas emission causes global warming and many environmental problems. Carbon dioxide is observed as one of the most important greenhouse gases; therefore, capture and storage (CCS) of $CO_2$ is considered a promising procedure for reduction of the greenhouse effects [1,2]. Hydrate formation is a well-known method to control $CO_2$ emission. Gas hydrates were first discovered during transport in pipelines [3]. The hydrate is a crystalline solid formed from a combination of gas and water molecules at reasonable operating conditions [4,5]. However, carbon dioxide hydrate formation is considered for its positive applications like gas sequestration process [6-8], transportation and gas storage [9,10] and cooling properties [11-13], but there are certain problems to be resolved before using $CO_2$ hydrate in any industrial applications. The problem includes high induction and growth time and low gas consumed mole and consumption rate.

Some studies reveal the effects of different surfactants [14-16], tetra-n-butyl ammonium bromide (TBAB) [17-19], and TBAB and cyclopentane (CP) [20-22] to solve the problem attribute of the process of $CO_2$ hydrate formation.

Addition of nanoparticles to the liquid phase is a novel way to improve the kinetics of gas hydrate formation. Due to the positive effect nanoparticles on the nucleation process, it has been observed that the presence of nanoparticles can reduce the induction time [23,24]. The simultaneous use of nanoparticles and surfactants can be more effective and reduce the induction time and increase storage capacity considerably [25,26]. Due to the positive effect of particles in increasing the mass transfer rate between the gas and liquid interface, the rate of hydrate formation will be increased. This causes a reduction in the growth time [27-29].

The specific surface area of nanoparticles can also play an important role in promoting the rate of hydrate formation. The results of experiments on four different nanoparticles showed that $SiO_2$ nanoparticles with the highest specific surface area had the greatest effect on the increase in the rate of carbon dioxide formation. However, silver nanoparticles with the lowest specific surface area did not affect the rate of hydrate formation [30]. Other investigators have claimed that the presence of hydrophilic functional groups on the surface of nanoparticles improves the rate of hydrate formation [31].

This study was carried out to propose a novel and efficient way to produce carbon dioxide hydrate with lower energy consumption. Due to the importance of the specific surface area and a hydrophilic group of the nanoparticles on hydrate formation kinetics, this study reports the effect of Boehmite (AlOOH) nanoparticles on the kinetics of the $CO_2$ hydrate formation process. Different kinetics parameters, such as induction time, growth time, and gas consumption rate, were measured to evaluate the hydrate formation procedure.

## EXPERIMENTAL

### 1. Materials

Carbon dioxide with a minimum purity of 99.9% was supplied from Arkan Gas Company, Iran. Sodium hydroxide and aluminum nitrate, obtained from Merck (Germany), were used to synthesize nanoparticles. The AlOOH nanoparticles were synthesized and used for the preparation of nanoparticle suspensions. The sus-

†To whom correspondence should be addressed.
E-mail: masoudrahimi@yahoo.com, m.rahimi@razi.ac.ir

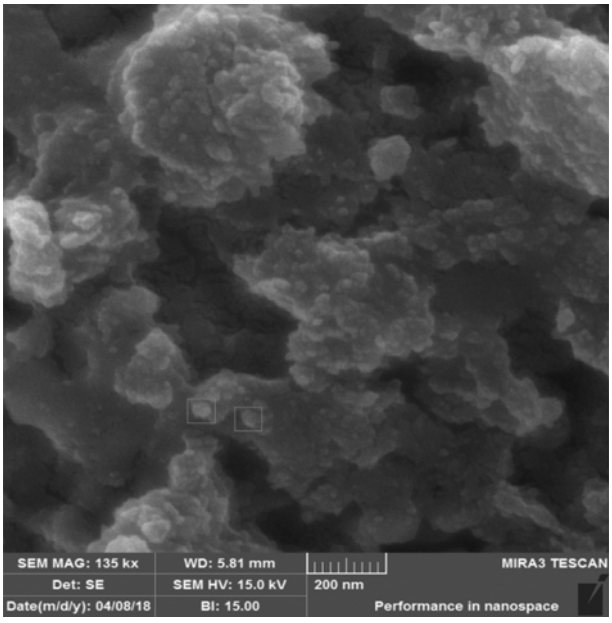


**Fig. 1. SEM image of the AlOOH nanoparticles.**

pensions were prepared by adding the nanoparticles to a specified amount of distilled water.

1-1. Synthesis and Characterization of AlOOH Nanoparticles

The AlOOH nanoparticles were synthesized by the following method: 20 ml of 3.25 M sodium hydroxide (NaOH) solution was added drop by drop to the 30 ml of 1.8 M aluminum solution ($Al(NO_3)_3 \cdot 9H_2O$) to form a milky mixture. The rate of addition was 2.94 ml/min under a constant rate of stirring for 17 min. The obtained mixture was sonicated in the ultrasonic bath at the room temperature for 3 h. The obtained precipitates were then filtered and washed with distilled water for several times, and finally placed in an oven at 220 °C for 4 h.

Fig. 1 shows an SEM photograph of the AlOOH nanoparticles. The unit cell of the Boehmite nanoparticle has a cubic orthorhombic structure [32]. According to Fig. 1, the mean dimension of the AlOOH nanoparticles is 20 nm. Moreover, the measured diffraction angles of nanoparticles by FTIR spectra were inconsistent with the standard pattern [32]. The results emphasize that the surface of the AlOOH nanoparticles is covered by the hydrophilic group of hydroxyl. The specific surface area of nanoparticles was calculated by BET adsorption equation. Accordingly, the specific surface area of AlOOH nanoparticles is 204 $m^2/g$.

## 2. The Experimental Apparatus

A schematic view of the $CO_2$ hydrate formation experimental apparatus is shown in Fig. 2. The main part of the system is a stainless steel reactor, where the hydrate formation process is taken placed. The total volume of the reactor is 300 $cm^3$ equipped with a data acquisition system. A vacuum pump evacuates the reactor. The pressures and temperatures of the reactor were recorded every 5 s. The liquid and gas phases were thoroughly mixed inside the reactor using a mechanical stirrer equipped with a four-blade impeller. The coolant circulator was used to control the temperature of the system by pumping the ethylene glycol solution through a jacket covering the reactor.

## 3. Procedure

A nanoparticle suspension containing different amount of AlOOH

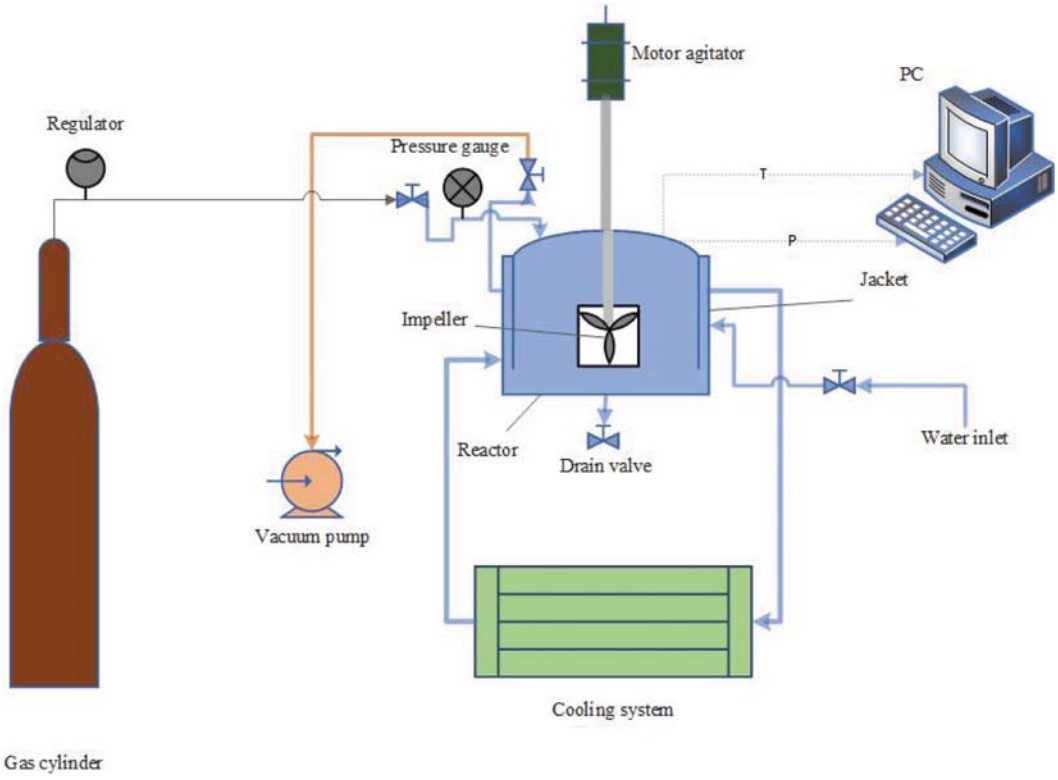


**Fig. 2. A schematic of the experimental apparatus.**

nanoparticles was prepared by using distilled water. Then, the nanoparticle suspension was sonicated in an ultrasonic bath for 30 min to disperse the nanoparticles in the solution uniformly. The nanoparticle suspensions were prepared in five different concentrations in the range between 25 and 200 ppm of the nanoparticles.

The reactor was carefully rinsed three times with distilled water. The fluid was then injected into the reactor by a vacuum pump and the air inside the reactor was discharged simultaneously. The cooling system was used to set the temperature of the reactor at the desired level. $CO_2$ was introduced to the reactor through the gas valve until the initial pressure reached the desired value. The solution was then agitated under a specified speed. The pressure inside the reactor started to decrease, as long as the system pressure reached the equilibrium point.

## MODEL AND CALCULATION METHODOLOGY

### 1. Gas Consumed Mole and Gas Consumption Rate

The amount of consumed mole during the hydrate formation process is calculated as follows:

$$\Delta n = \frac{P_0 V}{ZRT} - \frac{P_t V}{ZRT} \tag{1}$$

where, subscripts 0 and t indicate the initial and final condition, respectively. P, T, and V are pressure, temperature, the volume of gas inside the reactor, respectively. R and Z are the universal constants of gas and compressibility factor calculated by the Peng-Robinson equation of state [33,34].

The rate of consumed mole (R(t)) during the hydrate formation is calculated by the forward difference method [16] as follows:

$$R(t) = \left(\frac{d\Delta n_H}{dt}\right)_t = \frac{(n_{CO_2})_{t+\Delta t} - (n_{CO_2})_t}{\Delta t..n_{w0}} \tag{2}$$

where $(n_{CO_2})_t$ and $(n_{CO_2})_{t+\Delta t}$ are the mole number of $CO_2$ in the gas phase measured at t and t+Δt, respectively. The measurement interval (Δt) was 5 min. In Eq. (2), $n_{w0}$ is the initial mole of water inside the reactor.

### 2. First-order Model

The apparent rate constant of the first-order reaction is equal to the slope of the straight line (this is proved in section 4.3 of this study). The equation is shown below:

$$\frac{dC_h}{dt} = k(C - C_s) \tag{3}$$

$$\ln\frac{(C_0 - C_s)}{(C - C_s)} = kt \tag{4}$$

where k is the apparent rate constant, $C_h$ is the concentration of $CO_2$ in hydrate phase, C is the concentration of $CO_2$, $C_0$ is the initial concentration of carbon dioxide and $C_s$ is the concentration of $CO_2$ at the stationary point.

## RESULT AND DISCUSSION

### 1. Gas Consumption Rate

To ensure the reproducibility and accuracy of the obtained data, the experiments were performed three times, and the error bars were accordingly reported. Fig. 3 shows the amount of consumed mole of gas after the hydrate crystal formation for pure water and solutions with different concentrations of AlOOH nanoparticles. The results are presented as a function of time under the operating condition of 274.15 K, 29 bar and 100 rpm. As can be seen in the figure, there is a desirable concentration, which demonstrates the enhanced hydrate formation kinetics compared with other concentrations. Note that the desirable concentration is the best concentration obtained under the operating conditions of the current study. AlOOH nanoparticles were added to pure water with considering its desirable concentration, which was 50 ppm. This caused a considerable increase in the amount of gas consumption.

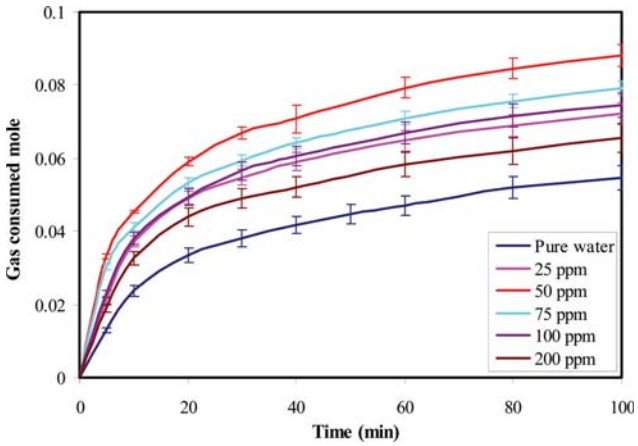


**Fig. 3. Effect of AlOOH nanoparticles on gas consumption during hydrate crystallization at an initial pressure of 29 bar and impeller speed of 100 rpm.**

It is assumed that the highest impact on the kinetics of carbon dioxide hydrate formation is observed in a certain range of nanoparticles concentrations. At lower concentrations, the presence of nanoparticles has a negligible effect on the improvement of mass transfer and heat transfer rate. However, at higher concentrations, the inter-particle interaction becomes stronger, which leads to agglomeration of nanoparticles and less Brownian motion.

A DLS test was conducted to determine the effect of the concentration of nanoparticles on their agglomeration in the aqueous phase. The experiments were at three different concentrations of 50, 200 and 2,000 ppm. Fig. 4 shows DLS analysis of nanoparticle suspension at different concentrations. In the DLS analysis of nanoparticles suspension of 50 ppm, a peak was centered at approximately 25 nm. However, as the concentration of nanoparticles increased to 200 ppm, a peak appeared at 180 nm. By increasing the suspension concentration to 2,000 ppm, the accumulation of nanoparticles was significantly increased, so a peak was centered at a higher point (825 nm).

Fig. 5 shows the effect of nanoparticles on the initial rate of hydrate formation at the mentioned operating conditions. The initial average rate of hydrate formation in the presence of 50 ppm AlOOH, was 0.0475 (mol of gas)/(mol of water·h), while for the pure water system was 0.019 (mol of gas)/(mol of water·h). However, the above results demonstrate all concentrations of nanopar-

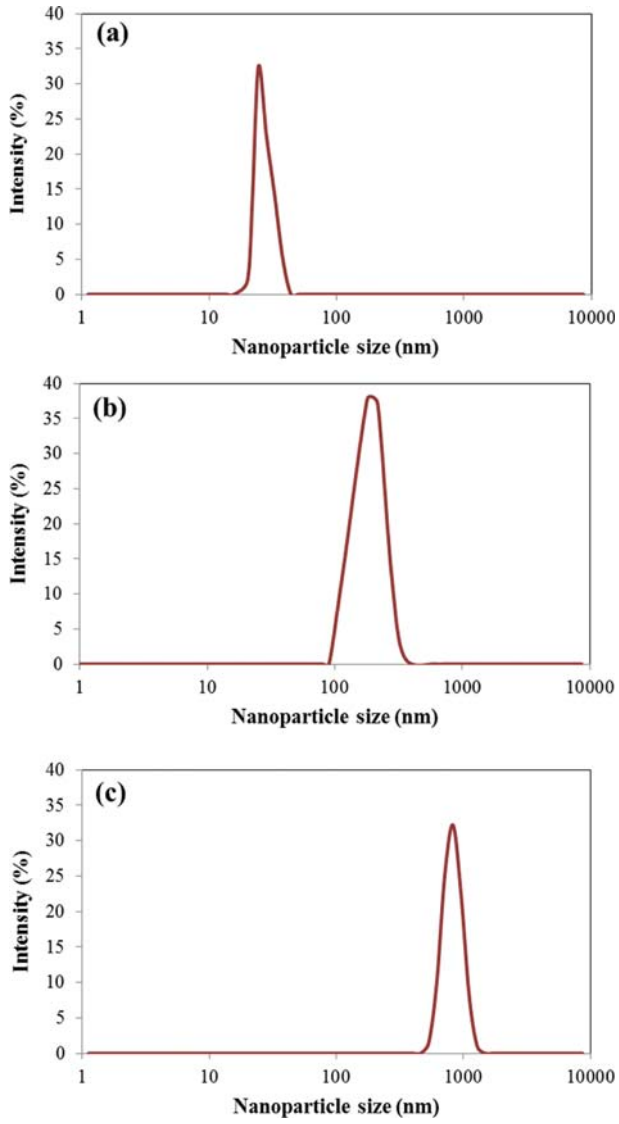


**Fig. 4. DLS analysis of nanoparticle suspension at different concentration of (a) 50 ppm, (b) 200 ppm and (c) 2,000 ppm.**

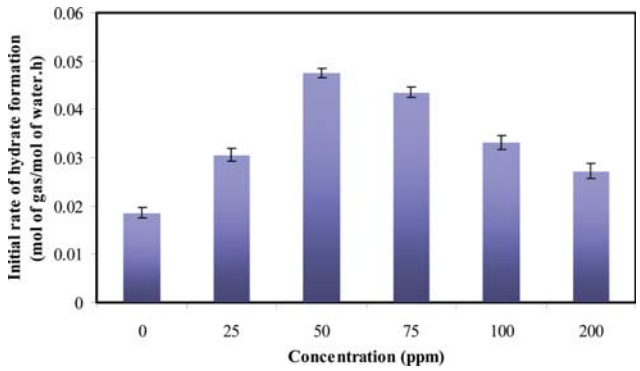


**Fig. 5. Effect of AlOOH nanoparticles at different concentrations on the initial rate of hydrate formation.**

ticles have a positive effect on $CO_2$ hydrate formation kinetics, but the rate of gas consumption at 50 ppm is considerably higher than other concentrations.

In the case of low soluble gases like $CO_2$, the mass transfer of gas molecule on the hydrate crystal surface plays an important role. Due to the high specific surface area, the addition of the nanoparticles to the liquid phase increased the mass and heat transfer between the gas-liquid-hydrate phases. Therefore, the amount of gas consumption rate can significantly increase in the presence of nanoparticles. Said et al. [30] employed different nanoparticles to study their impact on $CO_2$ hydrate formation kinetics. The obtained results showed that $SiO_2$ and Ag nanoparticles had the maximum and minimum surface area compared to the others. It was also observed that $SiO_2$ nanoparticles positively enhanced the gas consumption rate, while no significant effect was observed for Ag nanoparticles. Therefore, according to the past and the current research, it can be emphasized that the specific surface area of nanoparticles has a significant effect on the rate of carbon dioxide gas hydration formation.

Also, due to the exothermic nucleation process of hydrate formation, the nanoparticles with a high heat transfer coefficient accelerate the nucleation process and consequent growth of the hydrate crystals. Boehmite nanoparticles can dramatically increase the thermal conductivity of the fluid [35]. On the other hand, hydrophilic groups have a significant effect on the hydrate formation rate as the hydrophilic functional group leads to the persistence of particles in aqueous solution and prevents the accumulation of nanoparticles.

Improvement of gas absorption in the liquid phase in the presence of particles is expressed by different mechanisms. The first mechanism is the shuttle effect that was first presented by Kars et al. [36]. The presence of solid particles in the liquid-gas system increases the rate of gas absorption. In this phenomenon, the gas molecules are transferred from the gas-liquid interface to the liquid bulk. The gas molecules were absorbed on the solid particles, the particles then moved back to the bulk of the liquid phase, and were regenerated by desorbing the gas phase component. Another mechanism is a hydrodynamic effect in the gas-liquid boundary layer [37]. The diffusion boundary layer is reduced due to the collision of particles and the gas-liquid interface. Therefore, the particles intensify the mass transfer coefficient in the interface of the bubble and the liquid. These mechanisms imply an improvement in the mass transfer coefficient of gas and liquid in the presence of particles. It is very difficult to estimate quantitatively the effect of the shuttle and hydrodynamic effect mechanism on the $CO_2$ absorption. However, at low concentration of nanoparticle suspension, the impact of the shuttle effect mechanism is insignificant [38]. An increase in the nanoparticle concentration is expected to increase both shuttle effect and micro convections that lead to enhanced mass transfer rate [38,39]. It is concluded the hydrodynamic effect is a more reasonable mechanism than another effect to explain the mass transfer enhancement in nanoparticle suspensions. Fig. 6 illustrates the mechanism of the shuttle and hydrodynamic effect on gas absorption in the presence of solid particles.

Fig. 7 shows the amount of gas consumption rate at different initial gas pressure and the nanoparticle concentration of 50 ppm. As the figure reveals, the gas consumption rate depends on the initial pressure of $CO_2$, which directly relates to the initial amount of

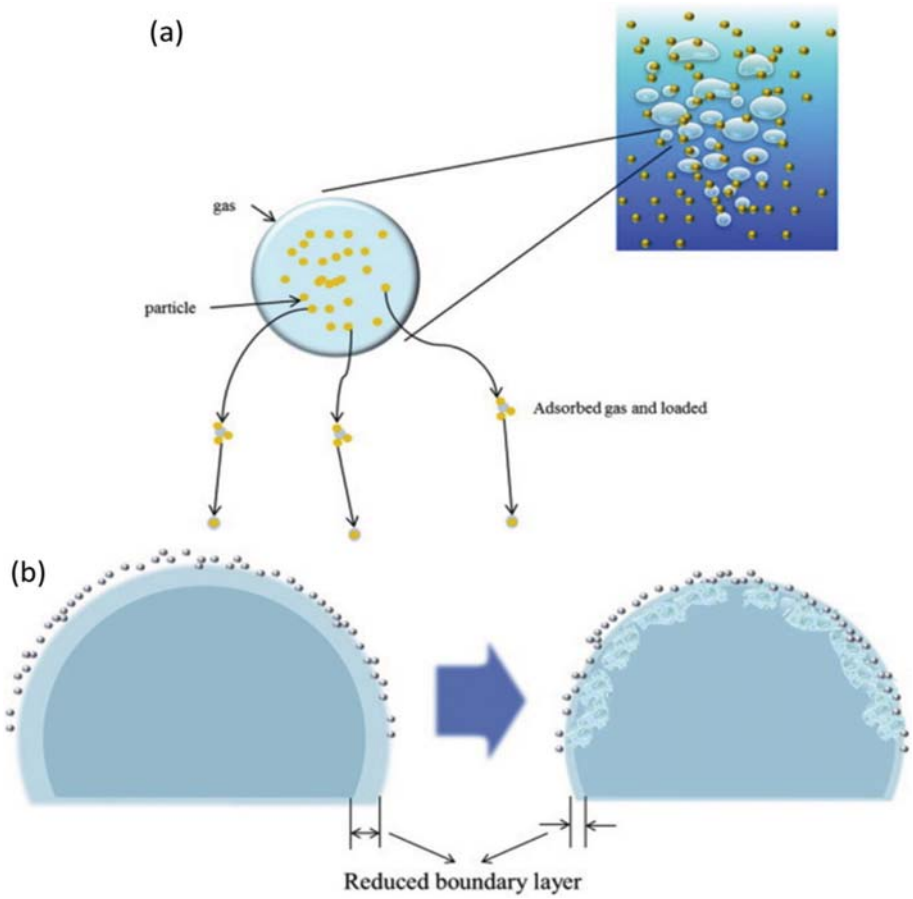


**Fig. 6. Absorption mechanism in the presence of particles: (a) shuttle effect; (b) hydrodynamic effect [38].**

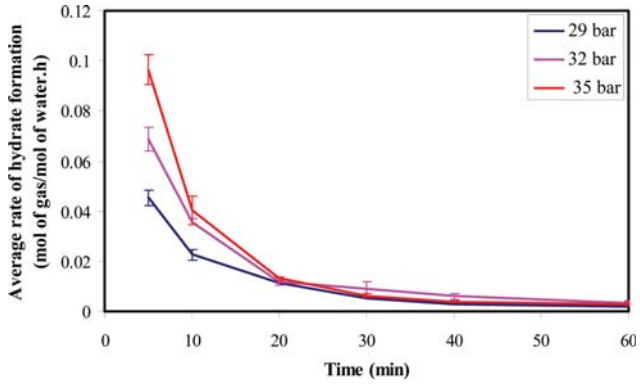


**Fig. 7. Effect of initial pressure on gas consumption rate in the presence of 50 ppm AlOOH.**

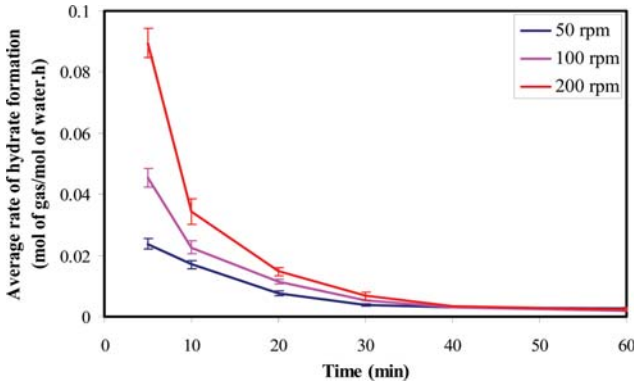


**Fig. 8. Effect of impeller speed on gas consumption rate in the presence of 50 ppm AlOOH.**

$CO_2$ in the system. In the primary minutes of the process, the initial rate of hydrate formation is significantly high for the higher initial pressures. Afterward, the rate of hydrate formation gradually becomes equal.

Comparison between the results of gas consumed mole and gas consumption rate in the initial times of the experiments shows approximately 72% and 115% enhancement in the case of 35 bar compared with 29 bar. Henry's Law can properly explain this phenomenon. Increasing the initial gas pressure of the system increases the partial pressure and, consequently, the rate of mass transfer. On the other hand, it is assumed that the trapping of $CO_2$ in the hydrate phase under high initial gas pressure strongly depends on the number of nucleation sites. However, at low initial pressure, a weak dependency occurred between the amounts of $CO_2$ uptake and the number of nucleation sites.

Effect of the impeller speed on $CO_2$ consumption rate during the crystallization process is shown in Fig. 8. The average initial rate of hydrate formation at 200 rpm and in the presence of 50 ppm

**Table 1. The average of induction time and growth time of $CO_2$ hydrate formation at different concentrations of AlOOH nanoparticles**

| Additives | Concentration (ppm) | Induction time (min) | Growth time (min) |
|---|---|---|---|
| Pure water | | 32.5±4.5 | 337±12 |
| AlOOH | 25 | 22.5±2.1 | 216±15.1 |
| | 50 | 6±0.5 | 180.5±9.5 |
| | 75 | 11.5±1.5 | 212.1±10.5 |
| | 100 | 23±3 | 220.2±10.1 |
| | 200 | 28±2.9 | 295.1±15 |

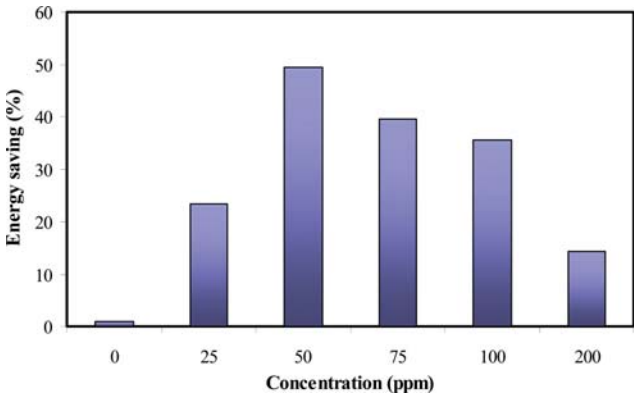


**Fig. 9. Comparison of energy saving for different concentrations of AlOOH nanoparticles.**

AlOOH was 0.0894. On the other hand, it can be seen that at 200 rpm the initial rate of hydrate formation was approximately four times higher than 50 rpm. Increasing the agitating intensity enhanced the mixing and the Reynolds number, which directly increased the mass transfer coefficient. This caused the observed enhancements in the gas consumption rate.

**2. Induction Time and Growth Time**

The experimental conditions and the results of induction and growth time in different concentrations of AlOOH at 29 bar and 100 rpm are represented in Table 1. The induction time and the growth time are determined by the temperature and pressure of the system. The process is carried out at a constant temperature. Induction time refers to the time from the beginning of the process to the moment when the system temperature raises abruptly. At this moment, the primary nuclei of hydrate are formed. On the other hand, the growth time is from the moment of the sudden rise in temperature until the pressure of the system reaches equilibrium pressure and remains constant. At first, both the induction and growth time have a desirable point, which is equivalent to the desirable point considered in the previous section. For pure water, as is listed in Table 1, the average induction time of $CO_2$ hydrate formation is about 32.5 min, while under the desirable concentration of AlOOH, 50 ppm, the relevant time is 6.00 min. On the other hand, the average growth time at the desired concentration of AlOOH is 180.5 min. So, the enhancement of induction time and growth time in the presence of AlOOH is 82.8 and 46.1%, respectively.

The above results show that AlOOH nanoparticles significantly reduce both induction and growth time. The reason for the decreased induction time may be explained as follows. Two types of nucleation in the hydrate formation process are recognized: heterogeneous and homogeneous nucleation. Homogeneous nucleation occurs in the bulk of this liquid phase when the crystal clusters are only in contact with the liquid phase. Heterogeneous nucleation is typically known faster than homogeneous nucleation. Heterogeneous nucleation takes place when the supersaturated liquid phase is in contact with other phases or molecular species. This type of nucleation can be found exclusively in gas hydrate systems. It is

**Table 2. Effect of different nanoparticles on energy saving of $CO_2$ hydrate formation process**

| Nanoparticle | Temperature (K) | Initial pressure (bar) | Energy saving (%) | Ref. |
|---|---|---|---|---|
| AlOOH | 274.15 | 29.0 | 47.2 | This work |
| AlOOH | 274.15 | 32.0 | 49.0 | This work |
| AlOOH | 274.15 | 35.0 | 47.1 | This work |
| Graphite | 277.0 | 35.0 | 0.0 | [23] |
| Graphene oxide | 275.15 | 30.0 | 5.0 | [27] |
| Graphene oxide | 275.15 | 30.0 | 0.0 | [27] |
| ZnO | 274.0 | 26.0 | 47.4 | [29] |
| ZnO | 274.0 | 32.0 | 0.0 | [29] |
| $Al_2O_3$ | 274.15 | 40.0 | 38.1 | [30] |
| $SiO_2$ | 274.15 | 40.0 | 23.8 | [30] |
| Cu | 274.15 | 40.0 | 0.0 | [30] |
| Ag | 274.15 | 40.0 | 0.0 | [30] |
| $Fe_3O_4$ | 276.15 | 30.6 | 12.0 | [40] |
| $Fe_3O_4$ | 274.15 | 30.1 | 12.1 | [40] |
| $Fe_3O_4$ | 276.15 | 35.2 | 11.7 | [40] |
| $Fe_3O_4$ | 274.15 | 35.4 | 14.2 | [40] |
| $Fe_3O_4$ | 274.15 | 40.6 | 28.9 | [40] |

because of contact with the particles and reactor wall. The inhomogeneity of the hydrate formation process can be increased in the presence of the particles, and therefore, a heterogeneous nucleation environment is provided. Thus, the induction time of the hydrate formation process is reduced. On the other hand, due to the positive effect of the specific surface area of the particles to increase the mass transfer between gas and liquid interface, the growth time is consequently reduced.

Comparison between different concentrations of AlOOH nanoparticles on energy saving is shown in Fig. 9. During the gas hydrate formation process, the total energy consumption is divided into the energy required to rotate the impellers and the energy of the cooling system. Therefore, by reducing the induction time and growth time in the presence of Boehmite nanoparticles, the overall energy consumption is also reduced significantly. According to obtained induction and growth time at 29 bar, 100 rpm, an energy saving of 47.2% is observed at a desirable concentration of 50 ppm. These results are very important in using $CO_2$ hydrates in industrial applications.

Table 2 shows a comparison between the amount of energy saving in terms of induction time and growth time in the current study with other research. As can be seen, under different operating conditions, Boehmite nanoparticles show a significant effect on the reduction of induction time and growth time and thus increase energy saving.

Fig. 10 demonstrates the effect of different initial pressure on induction time and growth time at 100 rpm and the nanoparticle concentration of 50 ppm. As illustrated, increasing the initial pressure of gas strongly decreases the induction time. The average amount of induction time for the pure water system and nanoparticle suspension of 50 ppm at 29 bar are 32.5 and 6.0 min, respectively. The average induction time for the pure water system and nanoparticle suspension system at 35 bar are 3.05 and 1.3 min, respectively. This shows that increasing the initial pressure from 29 to 35 bar decreases the amount of induction time about 90.5% and 78.3%, for the pure water system and nanoparticle suspension system. This is in agreement with previous research reported in the literature [23]. In that research, the authors also observed that increasing the initial pressure from 25 to 65 bar decreases the induction time about 37 and 57% for the pure water and suspension of graphite particles. No effect was found for the growth time.

Note that an increase in pressure of the system increases the liquid phase supersaturation. Therefore, the higher the initial pressure, the lower the required dissolved gas before the commencement of hydrate growth. Therefore, a higher initial pressure leads to a shorter induction time.

The amounts of induction time and growth time at different impeller speed are shown in Fig. 11. Increasing the agitating inten-

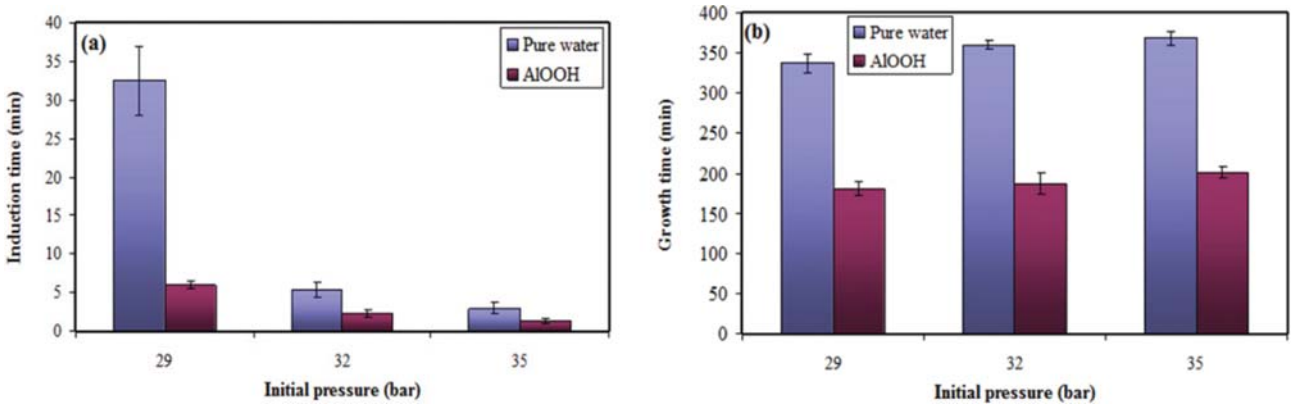


**Fig. 10. Effect of initial pressure on (a) induction time and (b) growth time at the impeller speed of 100 rpm.**

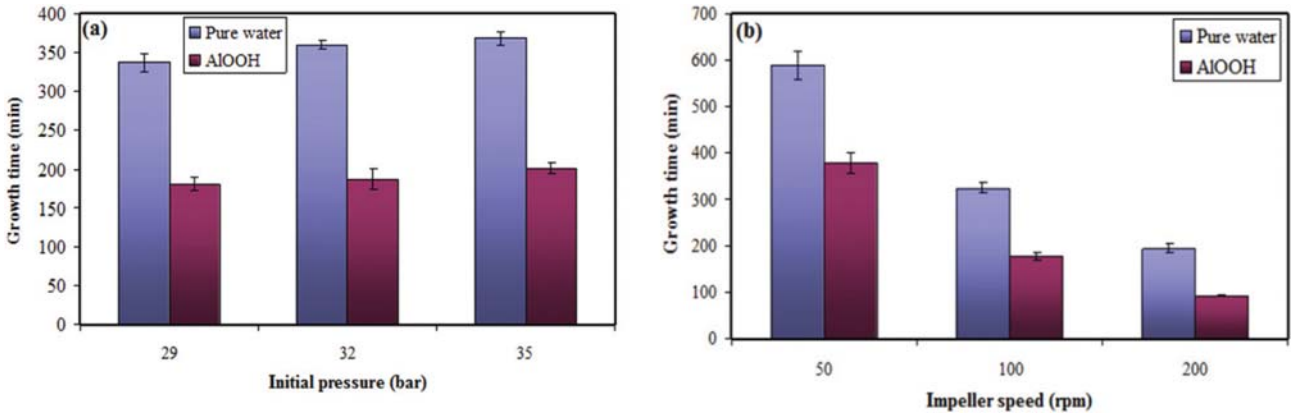


**Fig. 11. Effect of impeller speed on (a) induction time and (b) growth time at initial pressure of 29 bar.**

sity decreased both the induction and growth time significantly. On the other hand, according to statistical analysis for pure water and nanoparticle suspension systems, increasing the impeller speed from 50 to 200 rpm decreased both the induction time and growth time about 97% and 70%, respectively. Increasing the speed of the impeller increases the mass transfer coefficient between gas and fluid phases and therefore decreases the induction time. Thus, the induction time decreases to the lowest value by increasing the speed of impeller from 50 to 200 rpm. Increasing the impeller speed leads to a higher rate of supersaturation generation in the liquid phase and increases the rate of mass transfer through the gas-liquid interface. Therefore, the amount of the required $CO_2$ concentration to reach the onset of hydrate crystal decreases. Consequently, a higher agitating intensity leads to shorter induction time and growth time during the hydrate formation process.

### 3. Apparent Rate Constant

Fig. 12 depicts the effect of concentration of different particles on apparent rate constant during $CO_2$ hydrate crystallization. The figure reveals the results for the first 8 min of the experiments. Most of the hydrate crystal forms in this preliminary period. According to our observations, the apparent rate constant is maximum at $t=t_{ind}$ and then reaches a constant value for subsequent times. The apparent rate constant decreases at the end of the experiment and finally tends to its minimum value. The result of this phenomenon can be explained by the decrease in the rate of nucleation after the induction time, which leads to a decreased rate of gas consumption. As the figure shows, the addition of nanoparticles significantly increases the apparent rate constant. There are very good agreements between measured and predicted gas uptake with overall average absolute deviation (AAD) of 1.1%.

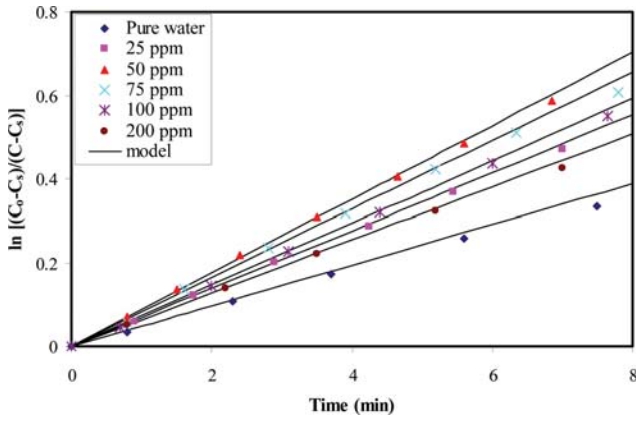


**Fig. 12. Effect of concentration of nanoparticle suspension on apparent rate constant of $CO_2$ hydrate formation.**

According to Figs. 9 and 12, there is a direct relation between the results of the apparent rate constant and the energy saving for different concentrations of nanoparticles. Any concentration that has a higher apparent rate constant, the energy savings at that concentration is also higher. So that the maximum amount of energy saving and the apparent rate constant are observed for 50, 75, 100, 25 and 200 ppm.

The calculated average apparent rate constants at different nanoparticle concentrations and operating condition are given in Fig. 13. For the suspension of the nanoparticle suspensions, increasing the concentration from 25 ppm to the desirable concentration of 50 ppm, the apparent rate constant is significantly increased. At higher nanoparticle concentrations, the maximum attainable of the apparent rate constant gradually decreased. It is justified by less Brownian motion, while the $CO_2$ effectively diffuses at the external surface of the crystals, and therefore the apparent rate constant decreases. It is quite clear that the kinetics of the process is significantly improved at 50 ppm of AlOOH nanoparticles suspensions. At these concentrations, the gas effectively diffuses into the liquid phase and consequently hydrate film significantly increases around the crystals. Therefore, a higher apparent rate constant can be obtained. It is also can be found that the initial pressure of the system can affect the apparent rate constant of the process. Increasing the initial pressure of $CO_2$ significantly increases the apparent rate constant because of the increased driving force of the system. In the different suspensions, the amount of apparent rate constant at 35 bar is approximately two-times bigger than that of 29 bar. Moreover, it is quite clear from Fig. 13 that the apparent rate constant depends on agitating intensity. As it was declared, increasing

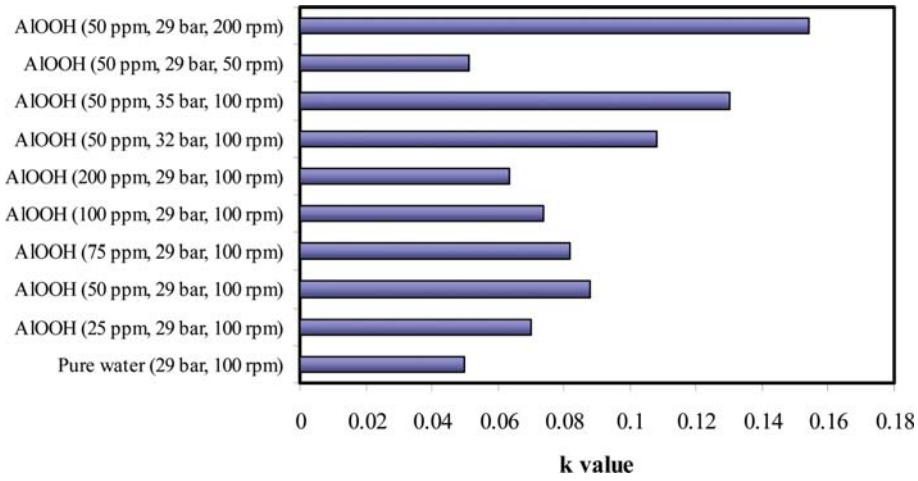


**Fig. 13. The average value of the apparent rate constant at different concentrations of AlOOH nanoparticles and different operating conditions.**

the agitating intensity increases the mass transfer rate between the gas and liquid phases. Therefore, the apparent rate constant at 200 rpm is approximately 3.5-times higher than that of 50 rpm.

## CONCLUSION

To produce $CO_2$ hydrate by a less energy consumption technique, the effects of using AlOOH nanoparticles on $CO_2$ hydrate formation kinetics were investigated. According to the results, the presence of nanoparticles had a remarkable impact on the induction time, growth time and gas consumption rate. It was seen that there is a desirable concentration, which is responsible for the most positive effect on the kinetics of the hydrate formation. The desirable concentration was found at 50 ppm for AlOOH nanoparticles. At this concentration, the most significant impacts on the hydrate formation process were observed. Besides, both the specific surface area and hydrophilic functional groups have a remarkable impact on promoting the hydrate formation process. Therefore, the nanoparticles of AlOOH with the specific surface area of 204 $m^2/g$ supported by hydrophilic hydroxyl group significantly impacted the kinetics of $CO_2$ hydrate formation. The results showed that at 50 ppm under 29 bar and 100 rpm, the gas consumption rate was 150% higher than that of pure water, while both the induction and growth time were decreased by 82.8% and 46.1%, respectively.

Also, $CO_2$ hydrate formation depends on the initial pressure of the gas. Increasing the pressure from 29 to 35 bar in the presence of 50 ppm AlOOH decreased the induction time about 70% and also increased the gas consumption rate of 115%. Also, increasing the agitating intensity decreased both the induction and growth time, while the gas consumption rate significantly increased. The results show that at 200 rpm, the initial rate of hydrate formation was 300% higher than that of 50 rpm. In addition, both the induction time and growth time decreased about 97 and 70% by increasing the speed of impeller from 50 to 200 rpm.

The proposed kinetics model was used for accurate description of $CO_2$ hydrate formation process at different initial pressures, impeller speeds, and particle concentrations. It was specified that the apparent rate constant depends on concentration, and it was maximum at the desirable concentration of 50 ppm. Moreover, the apparent rate constant became higher at higher initial pressure and agitating intensity.

## NOMENCLATURE

$P_0$ : initial pressure [MPa]
$P_t$ : final pressure [MPa]
V : volume of gas [$m^3$]
R : universal gas constant [$Jmol^{-1}K^{-1}$]
T : temperature [K]
R(t) : rate of gas consumed [mol $s^{-1}$]
$(n_{CO_2})_t$ : mole number of $CO_2$ in the gas phase measured at t
$(n_{CO_2})_{t+\Delta t}$ : mole number of $CO_2$ in the gas phase measured at t+Δt
t : time [s]
$n_{w0}$ : initial mole of water [mol]
$C_h$ : concentration of carbon dioxide in hydrate phase [mol $m^{-3}$]
C : concentration of carbon dioxide [mol $m^{-3}$]
$C_0$ : initial concentration of carbon dioxide [mol $m^{-3}$]
$C_s$ : concentration of $CO_2$ at the stationary point [mol $m^{-3}$]
k : apparent rate constant

### Greek Symbols

Δt : time difference [s]

## REFERENCES


1. P. Englezos and J. D. Lee, *Korean J. Chem. Eng.*, **22**, 671 (2005).
2. D. Kyung, K. Lee, H. Kim and W. Lee, *Int. J. GreenH. Gas Con.*, **20**, 285 (2014).
3. T. M. Guo, B. H. Wu, Y. H. Zhu, S. S. Fan and G. J. Chen, *J. Petrol. Sci. Eng.*, **41**, 11 (2004).
4. P. Englezos, *Ind. Eng. Chem. Res.*, **32**, 1251 (1993).
5. M. K. Chun and H. Lee, *Korean J. Chem. Eng.*, **13**, 620 (1996).
6. G. J. Moridis and E. D. Sloan, *Energy Convers. Manage.*, **48**, 1834 (2007).
7. J. W. Lee, P. Dotel, J. Park and J. H. Yoon, *Korean J. Chem. Eng.*, **12**, 2507 (2015).
8. J. W. Lee, K. K. Chun, K. M. Lee, Y. J. Kim and H. Lee, *Korean J. Chem. Eng.*, **19**, 673 (2002).
9. E. D. Sloan, *Ind. Eng. Chem. Res.*, **39**, 3123 (2000).
10. S. Almenningen, J. Gauteplass, P. Fotland, G. L. Aastveit, T. Barth and G. Ersland, *Int. J. GreenH. Gas Con.*, **79**, 272 (2018).
11. T. Mori and Y. H. Mori, *Int. J. Refrig.*, **12**, 259 (1989).
12. H. Inaba, *Int. J. Therm. Sci.*, **39**, 991 (2000).
13. E. D. Sloan and F. Fleyfel, *Fluid Phase Equilib.*, **76**, 123 (1992).
14. F. Pivezhani, H. Roosta and A. Dashti, *Energy*, **113**, 215 (2016).
15. A. Kumar, T. Sakpal and P. Linga, *Fuel*, **105**, 664 (2013).
16. B. ZareNezhad and V. Montazeri, *Energy Convers. Manage.*, **79**, 289 (2014).
17. X. Wang and M. Dennis, *Chem. Eng. Sci.*, **155**, 294 (2016).
18. N. N. Nguyen, A. V. Nguyen, K. T. Nguyen, L. Rintoul and L. X. Dang, *Fuel*, **185**, 517 (2016).
19. P. Babu, W. I. Chin, R. Kumar and P. Linga, *Energy Procedia*, **61**, 1780 (2014).
20. X. S. Li, C. G. Xu, Z. Y. Chen and H. J. Wu, *Energy*, **36**, 1394 (2011).
21. X. S. Li, C. G. Xu, Z. Y. Chen and J. Cai, *Int. J. Hydrogen Energy*, **37**, 720 (2012).
22. P. J. Herslund, K. Thomsen, J. Abildskov, N. Von Solms, A. Galfré, P. Brântuas and J. M. Herri, *Int. J. GreenH. Gas Con.*, **17**, 397 (2013).
23. S. D. Zhou, Y. S. Yu, M. M. Zhao, S. L. Wang and G. Z. Zhang, *Energy Fuels*, **28**, 4694 (2014).
24. S. Zhou, K. Jiang, Y. Zhao, Y. Chi, S. Wang and G. Zhang, *J. Chem. Eng. Data*, **63**, 389 (2018).
25. Y. S. Yu, C. G. Xu and X. S. Li, *J. Ind. Eng. Chem.*, **59**, 64 (2018).
26. A. Mohammadi, M. Manteghian, A. Haghtalab, A. H. Mohammadi and M. Rahmati-Abkenar, *Chem. Eng. J.*, **237**, 387 (2014).
27. B. ZareNezhad and V. Montazeri, *Petrol. Sci. Technol.*, **34**, 37 (2016).
28. J. W. Choi, J. T. Chung and Y. T. Kang, *Energy*, **78**, 869 (2014).
29. M. Mohammadi, A. Haghtalab and Z. Fakhroueian, *J. Chem. Thermodyn.*, **96**, 24 (2016).
30. S. Said, V. Govindaraj, J. M. Herri, Y. Ouabbas, M. Khodja, M. Belloum and R. Nagarajan, *J. Nat. Gas Sci. Eng.*, **32**, 95 (2016).
31. J. S. Renault-Crispo, S. Coulombe and P. Servio, *Energy*, **128**, 414

(2017).
32. V. Vatanpour, S. S. Madaeni, L. Rajabi, S. Zinadini and A. A. Derakhshan, *J. Membr. Sci.*, **401**, 132 (2012).
33. D. Y. Peng and D. B. Robinson, *Ind. Eng. Chem.*, **15**, 59 (1976).
34. K. M. Sabil, A. R. C. Duarte, J. Zevenbergen, M. M. Ahmad, S. Yusup, A. A. Omar and C. J. Peters, *Int. J. GreenH. Gas Con.*, **4**, 798 (2010).
35. N. Karami and M. Rahimi, *Int. J. Heat Mass Transf.*, **55**, 45 (2014).
36. R. L. Kars, R. J. Best and A. A. H. Drinkenburg, *Chem. Eng. J.*, **17**, 201 (1979).
37. J. H. J. Kluytmans, B. G. M. Van Wachem, B. F. M. Kuster and J. C. Schouten, *Chem. Eng. Sci.*, **58**, 4719 (2003).
38. J. H. Kim, C. W. Jung and Y. T. Kang, *Int. J. Heat Mass Transf.*, **76**, 484 (2014).
39. M. Jeong, J. W. Lee, S. J. Lee and Y. T. Kang, *Int. J. Heat Mass Transf.*, **108**, 680 (2017).
40. S. R. Firoozabadi, M. Bonyadi and A. Lashanizadegan, *J. Nat. Gas Sci. Eng.*, **59**, 374 (2018).